Battery Management System with Flying Capacitor Converter Operated in Discontinuous Current Mode

Taisuke Shioi, Mitsuru Miyashita, Satoshi Nagai,
Keisuke Kusaka, Jun-ichi Itoh
Dept. of Electrical, Electronics and Information Engineering
Nagaoka University of Technology
Niigata, Japan
shioi@stn.nagaokaut.ac.jp, miyashita@stn.nagaokaut.ac.jp
satoshi_nagai@stn.nagaokaut.ac.jp,
kusaka@vos.nagaokaut.ac.jp, itoh@vos.nagaokaut.ac.jp

Toshiki Nakanishi, Kazuhiro Kobayashi
Dept. of system development
San-Eisha, Ltd.
Tokyo, Japan
nakanishi-toshiki@san-eisha.co.jp,
kobayashi-kazuhiro@san-eisha.co.jp

***Abstract*— This paper proposes a novel battery management system (BMS) based on a three-level flying-capacitor three-port converter operated in discontinuous current mode (DCM). In BMS, the reduction of the inductor volume is required in a DC-DC converter. In particular, the proposed three-port converter contributes to the reduction of the inductor volume by sharing the inductor for the power conversion among solar cells, battery and DC-link. In addition, DCM is applied to further minimize the inductor volume. The validity of the proposed three-port converter and the inductor design for DCM operation is demonstrated with a 750-W prototype. In particular, it was mentioned that the prototype circuit achieves DCM in all operation modes. Furthermore, the inductor volume with DCM is reduced by 53 % compare to that with CCM.**

Keywords—Multi-port converter, Discontinuous current mode, DC-DC converter

I. Introduction

Recently, photovoltaics (PV) system has been actively applied to emergency power supply system to generate electricity during disaster [1]. However, generated electric power by PV system fluctuates due to the weather conditions. In order to absorb generated electric power fluctuation, auxiliary energy storage systems using batteries or double-layer capacitors are typically employed [2]-[3]. Therefore, battery management system (BMS) is required to control the power flow between the PV, the energy storage system, and an AC output side. In principle, BMS operated as DC-DC conversion which has two DC input ports and one DC output port. The DC input port is connected to PV panel and batteries, the DC output port is connected to single-phase inverter.

Conventional emergency power supply systems, which is consist of a single-phase inverter and two DC-DC converters operating as PCS for PV and BMS, is introduced in [4]. The conventional BMS results in a large volume due to two boost inductors in the DC-DC converters. The Reduction of the number of inductors is required in order to minimize the circuit volume. Hence, multi-port converters have been actively researched to reduce the circuit volume [5-8]. In ref.[6], the multi-port converter achieves the bidirectional power flow between two DC input ports by using only one converter. However, two inductors are still necessary for two input ports. In ref.[7], the bidirectional operation is achieved by two inductors. Furthermore, this multi-port converter might not be achieved the reduction of inductor volume because these multi-port converter requires large inductance due to the operation of Continuous Current Mode (CCM). In ref.[8], reduction of the number of inductors is achieved by connecting each DC input port in series. However, the problem of this circuit is that it cannot convert power between two DC input ports. Therefore, this multi-port converter is inapplicable to BMS which requires the energy charge to the battery from PV is required. Thus, it is required to reduce the inductor volume by decreasing inductance and number of inductors, while realizing the bidirectional power conversion between battery and PV.

This paper proposes a novel multi-port converter based on the Flying Capacitor Converter (FCC) [9] topology to reduce of inductor volume. The battery is connected to the low voltage port of FCC and PV is replaced with the flying capacitor in the proposed three-port converter. The circuit volume is reduced because the power conversion between PV and battery uses only one inductor. In addition, Discontinuous Current Mode (DCM) [10-11] is applied to further reduce inductance. Moreover, the power conversion from PV to DC-link without battery is also achieved by time-sharing technique. The originality of this paper is that 1) FCC is used as three-port converter, 2) the DCM operation is employed with the FCC topology to achieve the bidirectional power flow among PV, the battery and the DC-link while using only one inductor.

This paper is organized as follows; first, the descriptions of the circuit configuration and the circuit operation are introduced. Secondly, the design method of the inductor to operate the DCM is derived. In addition, the inductor volume comparison between DCM and CCM is discussed. Finally, the operation of the three-port converter is demonstrated with a 750-W prototype. It is mentioned that the three-port converter achieves each mode operation and DCM control. Furthermore, it is also obtained that the inductor volume is reduced by 53 % with DCM compare to CCM.

II. Circuit Configuration and Operation Mode

A. Configuration of conventional circuit

Fig. 1 shows a conventional emergency power supply system. The conventional system is composed by a single-phase inverter and two DC-DC converters operating as BMS and PCS for PV. A large volume is required in the conventional system due to two boost inductors in the DC-DC converters. Both the number of inductors and the inductance value should be reduced to minimize the inductor volume.

B. Configuration of proposed three-port converter

Fig. 2 shows the configuration of the proposed three-port based on three-level FCC. The battery is connected to the FCC low voltage port and the PV is connected to the flying capacitor nodes. The circuit volume is reduced because there is only one inductor in this system. Furthermore, the number of switching devices does not increase compared to the conventional circuit shown in Fig. 1. The proposed three-port converter uses the switching devices which the voltage rating is half of those in the typical boost converter because of the series connection of four switches. The volume of the inductor is further reduced due to the low inductance of the boost inductor with the DCM application. Note that the proposed three-port converter achieves zero current switching(ZCS) because the inductor current falls to zero before turning ON in DCM.

C. Operation modes of proposed three-port converter

Fig. 3 shows each operation modes of the three-port converter. The three-port converter has four operation modes according to the power flow.

1) Mode I(Fig.3(a)): The power flow of Mode I is from the battery to DC-link. In this mode, the three-port converter operates as the boost converter. The current flows through either the two series MOSFETs or two series body diodes depending on the switching modes: synchronous switching operation or asynchronous switching operation. Note that this mode achieves biderectional operation.

2) Mode II(Fig.3(b)): The power flow of Mode II is from the battery and PV to DC-link. In this mode, the three-port converter operates as the FCC discharging the flying capacitor. That is the power is sending from PV to DC-link. Similarly, the current flows through either the switches S_1 by the synchronous switching operation or the asynchronous switching operaion with body diode.

3) Mode III(Fig.3(c)): The power flow of Mode III is from PV to the battery. In this mode, the three-port converter operates as the buck converter. Similarly, the current flows through either the switches S_3 and S_4 by the synchronous switching operation or the asynchronous switching operaion with body diode

4) Mode IV(combination of Mode II and Mode III): The power flow of Mode IV is from PV to DC-link, combining Mode II and Mode III. First, the power from PV is temporarily transferred to the battery by Mode III. Next, this power outputs to DC-link through Mode II. Thus, the direct power flow from PV to DC-link is achived by the combination of Mode II and Mode III. Note that the battery does not charge or discharge in Mode IVbecause the energy from PV is temporarily stored in the filter capacitor which is connected in parallel to the battery. In practical, the power flows from PV to DC-link and charge battery from PV are also achieved by the current ratio of Mode II and the Mode III in Mode IV.

Table I lists the switching pattern and the power flow of each mode. Note that the asynchronous switching operation is employed to evaluate the basic operation. In Table I, ON describes the on-state of the switch, whereas OFF describes the off-state of the switch, and Duty describes the switching operation with duty ratio of the switch. In addition, S_1 is employed by either a switch or a diode because switch S_1 is always OFF in Table. I.

III. CONTROL METHOD AND INDUCTOR DESIGN

Proposed three-port converter applies the DCM operation. In this section, the duty ratio calculation is explained. In addition, the inductor volume calculation is mentioned to clarify the validity of the proposed circuit. Finally, the control diagram of the three-port converter is introduced.

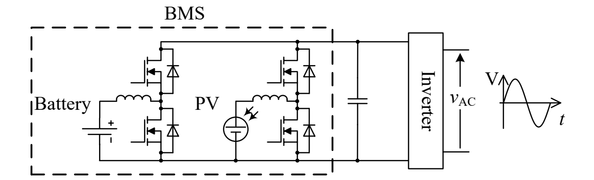

Fig. 1. Conventional battery management system using two chopper.

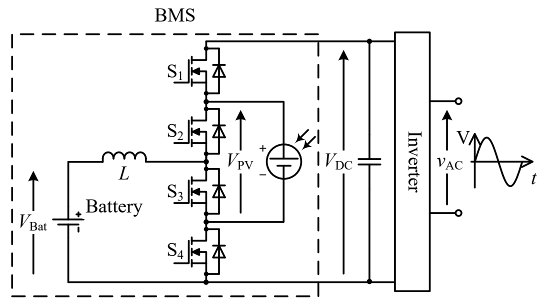

Fig. 2. Proposed three-port converter circuit based on three-level FCC.

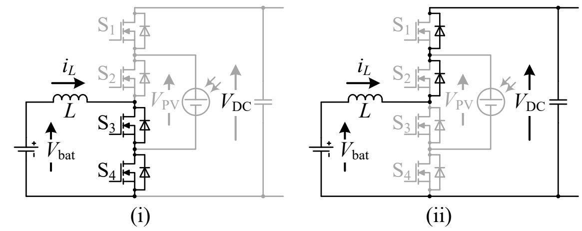

(a) Mode I : power flow From battery to DC-link.

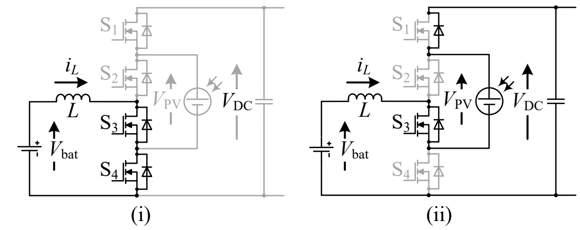

(b) Mode II : power flow From battery and PV to DC-link.

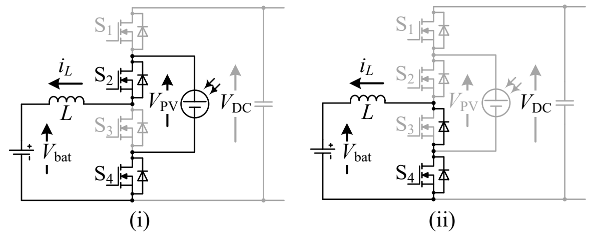

(c) Mode III : power flow From PV to the battery.

Fig. 3. Operation modes of the three-port converter. The power flow from PV to DC-link (Mode IV) is achieved combining Mode II and III.

Table. I. Switching pattern in each modes.

	S_1	S_2	S_3	S_4	Power flow
Mode I	OFF	OFF	ON	Duty	Battery → DC link
Mode II	OFF	OFF	Duty	Duty	PV+Battery → DC link
Mode III	OFF	Duty	OFF	ON	DC link → Battery
Mode IV	OFF	OFF	Duty	Duty	PV → DC link
	OFF	Duty	OFF	ON	

A. Derivation of duty ratio

Fig. 4 shows the inductor current waveform in DCM including zero-current interval. In this section, the duty ratio is obtained from the average inductor current i_{Lave}, inductor peak current i_{pk}, battery voltage V_{bat}, PV voltage V_{PV}, and DC-link voltage V_{DC}.

1) Duty ratio of Mode I: In Mode I, the interval $D_{1\_m1}T_{sw}$ is for Mode I(i) in Fig. 3(a), whereas the interval $D_{2\_m1}T_{sw}$ is Mode I(ii) in Fig. 3(a). The duty ratio D_1 is calculated from average inductor current I_{Lave}. Circuit equation in Mode I(i) and Mode I(ii) are represented as

$$\begin{cases} V_{L\_D1\_m1} = V_{bat} = L\dfrac{di_L}{dt} \\ V_{L\_D2\_m1} = V_{DC} - V_{bat} = L\dfrac{di_L}{dt} \end{cases} \tag{1}$$

where i_L is the inductor current, V_{bat} is the battery voltage, and V_{DC} is the DC-link voltage. Then, the inductor peak current I_{pk} is given by (2) from (1).

$$\begin{cases} I_{pk} = \dfrac{V_{bat}}{L} D_{1\_m1}T_{sw} \\ I_{pk} = \dfrac{V_{DC} - V_{bat}}{L} D_{2\_m1}T_{sw} \end{cases} \tag{2}$$

where T_{sw} is the switching period, D_{1_m1} is the duty ratio during the inductor charge period, and D_{2_m1} is the duty ratio during the inductor discharge period. The average inductor current i_{Lave} is obtained by averaging the inductor current during the switching period. The average inductor current is calculated by the inductor peak current I_{pk}, the duty ratio D_{1_m1}, D_{2_m1}, and the switching period T_{sw} in Fig. 4. The average inductor current is given by (3)

$$I_{Lave} = \frac{1}{2} I_{pk} \times (D_{1\_m1} + D_{2\_m2}) \tag{3}$$

The duty ratio D_{1_m1} of the inductor energy charge interval in Mode I is calculated from on (2) and (3). The duty ratio D_{1_m1} is given by (4).

$$D_{1\_m1} = \sqrt{\frac{2LI_{Lave}}{T_{sw}V_{bat}} \frac{V_{DC} - V_{bat}}{V_{DC}}} \tag{4}$$

The duty ratio D_{2_m1} of the inductor energy discharge interval in Mode I is calculated from (2) and (3).The duty ratio D_{2_m1} is given by (5).

$$D_{2\_m1} = \sqrt{\frac{2LI_{Lave}}{T_{sw}V_{DC}} \frac{V_{bat}}{V_{DC} - V_{bat}}} \tag{5}$$

Both duty ratios D_{1_m1} and D_{2_m1} are calculated from the average inductor current I_{Lave} that is command value. In the Mode I, the average inductor current I_{Lave} is controlled by switching S_3 and S_4 from (4).

2) Duty ratio of Mode II: The duty ratio of Mode II is for calculated by similar method as Mode I. The interval $D_{1\_m2}T_{sw}$ is Mode II(i) in Fig. 3(b). The interval $D_{2\_m2}T_{sw}$ and zero current interval is Mode II(ii) in Fig. 3(b). The inductor peak current of Mode II is given by (6) based on faraday's law.

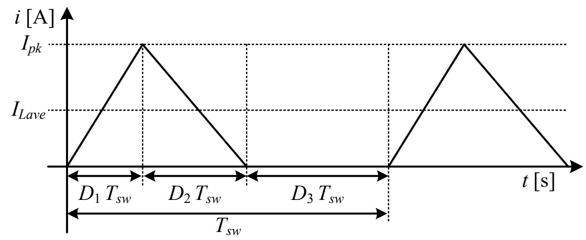

Fig. 4. Inductor current waveform with DCM.

$$\begin{cases} I_{pk} = \dfrac{V_{bat}}{L} D_{1\_m2}T_{sw} \\ I_{pk} = \dfrac{V_{DC} - V_{PV} - V_{bat}}{L} D_{2\_m2}T_{sw} \end{cases} \tag{6}$$

where V_{PV} is the voltage of the PV. The duty ratio D_{1_m2} and D_{2_m2} are given by (7) and (8) from (3) and (6).

$$D_{1\_m2} = \sqrt{\frac{2LI_{Lave}}{T_{sw}V_{bat}} \frac{V_{DC} - V_{PV} - V_{bat}}{V_{DC} - V_{PV}}} \tag{7}$$

$$D_{2\_m2} = \sqrt{\frac{2LI_{Lave}}{T_{sw}} \frac{V_{bat}}{(V_{DC} - V_{PV})(V_{DC} - V_{PV} - V_{bat})}} \tag{8}$$

3) Duty ratio of Mode III: The duty ratio of Mode III is calculated by similar method as Mode I. The interval $D_{1\_m3}T_{sw}$ is Mode III(i) in Fig. 3(c). The duty ratio $D_{2\_m3}T_{sw}$ and zero current interval is Mode III(ii) in Fig. 3(c). The inductor peak current in Mode III is given by (9).

$$\begin{cases} I_{pk} = \dfrac{V_{PV} - V_{bat}}{L} D_{1\_m3}T_{sw} \\ I_{pk} = \dfrac{V_{bat}}{L} D_{2\_m3}T_{sw} \end{cases} \tag{9}$$

The duty ratio D_{1_m3} and D_{2_m3} are given by (10) and (11) from (3) and (9).

$$D_{1\_m3} = \sqrt{\frac{2LI_{Lave}}{T_{sw}V_{PV}} \frac{V_{bat}}{V_{PV} - V_{bat}}} \tag{10}$$

$$D_{2\_m3} = \sqrt{\frac{2LI_{Lave}}{T_{sw}V_{PV}} \frac{V_{PV} - V_{bat}}{V_{bat}}} \tag{11}$$

B. Derivation of average inductor current and power

In this section, the average inductor current is calculated to obtain the desired output power. Note that the conversion loss is neglected for the sake of simplicity.

1) Output power of Mode I : The power flow of Mode I is from the battery to DC-link. Therefore, the relationship of the average inductor current I_{Lave} and the output power P_{out1} is given by (12).

$$I_{Lave} = \frac{P_{out1}}{V_{bat}} \tag{12}$$

The average inductor current is decided by the desired output power.

2) Output power of Mode II : The power flow of Mode II is from the battery and PV to DC-link. Therefore, the relationship of the input power and the output power is given by (13)

$$P_{out2} = P_{bat} + P_{PV} \tag{13}$$

where P_{out2} is the output power to DC-link, P_{bat} is the power from the battery, and P_{PV} is power from PV. The power of PV is given by (14) and the power of battery is given by (15).

$$P_{PV} = V_{PV}\frac{P_{out2}}{V_{DC}} \tag{14}$$

$$P_{bat} = V_{bat}I_{Lave} \tag{15}$$

Next, the relationship between the average inductor current I_{Lave} and the output power P_{out2} is given by (16) from (13), (14) and (15).

$$I_{Lave} = \frac{P_{out2}}{V_{bat}}\left(1-\frac{V_{PV}}{V_{DC}}\right) \tag{16}$$

3) Output power of Mode III : The power flow of Mode III is from PV to the battery. Therefore, the average inductor current i_{Lave} is derivated by the power of battery P_{out3}. The relationship between the average inductor current I_{Lave} and output power P_{out3} is given by (17)

$$I_{Lave} = \frac{P_{out3}}{V_{bat}} \tag{17}$$

4) The inductor current required in Mode IV : Fig. 5. shows the inductor current waveform in Mode Ⅳ. Mode Ⅳ outputs the power to DC-link from only PV by combining Mode Ⅱ and Mode Ⅲ. The control period becomes two times longer than that in other modes due to the combination of two modes. In the control period, the DC-link receives the power only during Mode Ⅱ. Therefore, the relationship between Mode Ⅱ and Mode Ⅳ is given by (18).

$$P_{out2} = 2P_{out4} \tag{18}$$

In Mode Ⅳ, the double value of the desired power P_{out4} is required in Mode II. In addition, the output power of the battery in Mode II is charged by Mode III. Therefore, the relationship of the power P_{out2} and P_{out3} is given by (19) from (13)

$$P_{out2} = P_{out3} + P_{PV} \tag{19}$$

Therefore, the average inductor current I_{Lave} which is required to obtain the output power P_{out2} is given by (20) based on (16), (17), (18) and (19).

$$\begin{cases} I_{Lave} = \dfrac{2P_{out4}}{V_{bat}}\left(1-\dfrac{V_{PV}}{V_{DC}}\right), (@Mode2) \\ I_{Lave} = -\dfrac{2P_{out4}}{V_{bat}}\left(1-\dfrac{V_{PV}}{V_{DC}}\right), (@Mode3) \end{cases} \tag{20}$$

Note that the direction of the inductor current is defined as positive when it flows from the battery. The inductor current becomes negative in Mode III because current flows into the battery from PV. In order to satisfy (21), the inflowing current to the battery in Mode III is required to be equal to the current which is output from battery in Mode II.

In each modes, the average inductor current which is the command value of duty ration is decided from the output power based on (13), (17), (18) and (21), respectively. Therefore, the desired output power is obtained by controlling the average inductor current based on these equations.

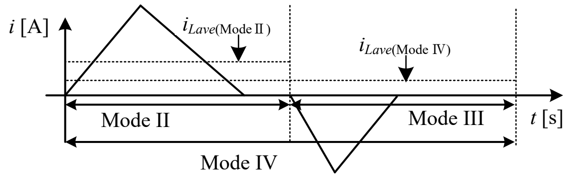

Fig. 5. Inductor current waveform in Mode IV.

C. Design of inductance

The inductance should be designed properly to ensure the DCM operation. In particular, the minimum inductance provides Boundary Conduction Mode (BCM) operation with rated current rms value.

1) Design of inductance in Mode Ⅰ: In order to achieve DCM, $D_{1\_m1}T_{sw}+D_{2\_m1}T_{sw}$ should be smaller than T_{sw}. The condition for the achievement of BCM is given by (21) from (4) and (5).

$$D_{1\_m1} + D_{2\_m1} = \sqrt{\frac{2LI_{Lave}}{T_{sw}V_{bat}}\frac{V_{DC}}{V_{DC}-V_{bat}}} \le 1 \tag{21}$$

In Mode I, the inductance L which achieves DCM is given by (22) from (21).

$$L \le \frac{T_{sw}V_{bat}(V_{DC}-V_{bat})}{2I_{Lave}V_{DC}} \tag{22}$$

2) Design of inductance in ModeII: The inductance to achieve BCM in the Mode II is calculated by similar method as Mode I. The condition of inductor current achieving the BCM is given by (23) from (7) and (8).

$$D_{1\_m2} + D_{2\_m2} = \sqrt{\frac{2LI_{Lave}}{T_{sw}V_{bat}}\frac{V_{DC}-V_{PV}}{V_{DC}-V_{PV}-V_{bat}}} \le 1 \tag{23}$$

In Mode II, the inductance L which achieves DCM is given by (24) from (23).

$$L \le \frac{T_{sw}V_{bat}(V_{DC}-V_{PV}-V_{bat})}{2I_{Lave}(V_{DC}-V_{PV})} \tag{24}$$

3) Design of inductance in Mode III: The inductance to achieve BCM in the Mode III is calculated by similar method as Mode I. The condition of inductor current achieving BCM is given by (25) from (10) and (11).

$$D_{1\_m3} + D_{2\_m3} = \sqrt{\frac{2LI_{Lave}}{T_{sw}V_{bat}}\frac{V_{PV}}{V_{PV}-V_{bat}}} \le 1 \tag{25}$$

In Mode III, the inductance L which achieves DCM is given by (26) from (25).

$$L \le \frac{T_{sw}V_{bat}(V_{PV}-V_{bat})}{2I_{Lave}V_{PV}} \tag{26}$$

The inductance condition is considered in BCM in each mode. The minimum inductance among modes is selected to achieve DCM. On the other hand, the inductor peak current will be increased if the inductance is designed as smaller value. Thus, the lower limit of inductance is decided by the maximum current rating of the semiconductor device and the saturation magnetic flux density of the core.

D. Calculation of inductor volume

In this section, the inductor volume is estimated in terms of inductor storage energy. The inductor volume is given by (27) based on Area Product concept [12].

$$Vol_L = K_V \left(\frac{2W}{K_u B_m J_w} \right)^{\frac{3}{4}} \tag{27}$$

where K_V is the coefficient which depends on the shape of core, W is inductor energy, K_u is the window utilization factor, B_m is the maximum flux density, and J_m is the current density. The inductor volume is proportional to the three-fourths of the inductor storage energy. Therefore, the reduction ratio of the inductor volume is obtained by comparing the inductor storage energy between DCM and CCM.

Next, the inductor energy in CCM which is the target for comparison is calculated. Note that the ripple ratio of inductor current in CCM is assumed as peak-to-peak 30%. In CCM, The inductance to achieve CCM is given by (28) in consideration of the current ripple ratio.

$$L = \frac{V_{bat}}{\Delta I_L f_{sw}} \frac{V_{DC} - V_{bat}}{V_{DC}} \tag{28}$$

where ΔI_L is the current ripple. The inductor storage energy is calculated from inductor peak current. The inductor volume is compared in next chapter according to the experimental conditions.

E. Control block diagram

Fig. 6 shows the control block diagram of the three-port converter which is applied with DCM. The control block diagram consists of the duty selector, a PWM generator and a switching pattern selector. The duty ratio is calculated based on the mode select signal and the command average inductor current. Next, the PWM signal is generated based on the mode selector signal and the duty ratio. Note that the applied switch is decided by the mode selector signal as shown in the Table 1. Furthermore, the gate interruption is added to protect the circuit. In this paper, the inductor current is generated by open-loop control based on (12), (16) and (17).

IV. EXPERIMENTAL RESULTS

A. Design method of prototype

Table II lists the experimental conditions. The proposed three-port converter operation with DCM is demonstrated with a 750-W prototype. In this paper, DC-link of 150 V is selected with the single-phase AC 100 V. In the experiment, the battery and PV are replaced by the DC power supplies. The inductance is designed with the consideration of 1.2 times higher rating power by (22), (24) and (26) to achieve DCM. In particular, DCM is achieved by the inductance of under 32.0 μH in Mode I, 43.5 μH in Mode II, and 30.0 μH in Mode III. Therefore, the inductance is required to lower than 30.0 μH to achieves DCM in all mode. In the experiment, the inductance of 14.5 μH is selected to achieves DCM. Note that the inductance is measured from the inductor current gradient at the average value of 15 A.

B. Comparison of inductor volume

The inductor volume is obtained by substituting the parameter in Table 2 into (1) and (28). The inductor peak current in DCM is 60.2 A from (2), whereas the inductor peak current in CCM is 20.5 A. In addition, the inductance in DCM is 14.5 μH, whereas the inductance in CCM is 340 μH from (28). Hence, the inductor energy in DCM is 26.1 mJ, and the inductor energy in CCM is 71.4 mJ from (27). Consequently, the inductor volume of the proposed circuit with DCM is reduced by 53%.

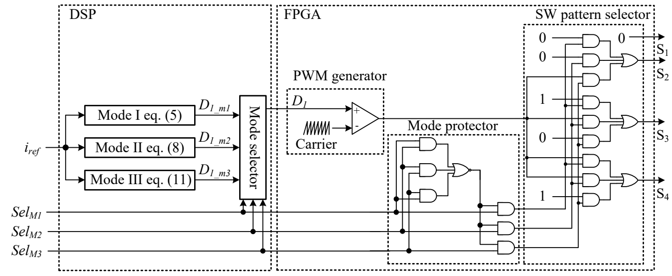

Fig. 6. Control block diagram of FCC with DCM.

Table II. Experimental conditions.

Parameter	Symbol	Value
Output power	P_{out}	750 W
Output voltage	V_{DC}	150 V
Battery voltage	V_{bat}	48 V
PV voltage	V_{PV}	90 V
Boost up inductor	L_1	14.5 μH
Battery decoupling capacitor	C_{bat}	1500 μF
PV decoupling capacitor	C_{PV}	1500 μF
DC link decoupling capacitor	C_{DC}	650 μF
PWM Carrier Frequency	f_{sw}	20 kHz
Mode I current command	I_{ref1}	15.8 A
Mode II current command	I_{ref2}	8.0 A
Mode III current command	I_{ref3}	14.1 A
Mode IV current command	I_{ref4}	16.1 A

C. Evaluation of operation waveform

Fig. 7 shows the operation waveforms in Mode I. In Mode I, the power is transferred from the battery to DC-link. Thus, in this mode, the three-port converter operates as same as the boost converter. It is mentioned that the inductor current achieves DCM as shown in Fig. 7. The average inductor current is 15.2 A which is 3.8% lower than the current command of 15.8 A. This error occurs due to the switching loss and conduction loss of the switching devices. Note that the output power error is not occur due to the dead time because proposed circuit does not have switches which need inverse duty.

Fig. 8 shows the operation waveforms in Mode II. In Mode II, the power is output from PV and the battery to DC-link. Fig. 8 mentioned that the inductor current achieves DCM. The average inductor current is 6.1 A which is 23.6% lower than the current command of 8 A. The inductor current error of Mode II is larger than Mode I. The conduction route is different in each modes; therefore, the inductor current error is different due to the also difference of the conduction loss.

Fig. 9 shows operation waveforms in Mode III. In Mode III, the battery is charged by PV. It is mentioned that the inductor current achieves DCM as shown in Fig. 9. In addition, the inductor current is negative because the direction of inductor current is inverse to Mode I and Mode II. The average inductor current is -12.3 A which is 23.6% lower than current command of -16.1 A. The reason of the error is same as mentioned in above paragraph.

Fig. 10 shows the operation waveforms in Mode IV. In Mode IV, the power is output from PV to DC-link by operating alternately between Mode II and Mode III. Note that the inductor current is negative in Mode III, whereas the current direction is different from Mode II because the current flows from PV to the battery. Theoretically, the average inductor current should become 0 A because the current command of the average inductor current in Mode II and Mode III are equal. However, the average inductor current is -1.6 A in Mode IV in the experiment. This current error occurs from the loss difference between Mode II and Mode III.

V. CONCLUSION

In this paper, the three-port converter based on the flying capacitor converter was proposed. The three-port converter reduced the inductor volume by 53% with the sharing use of the inductor and the application of DCM. The duty ratio and the inductance of the three-port converter were calculated to achieve DCM. The validity of the calculation method of the duty ratio and the inductance was demonstrated with the 750-W prototype.

As the future works, improvement of the circuit efficiency by synchronous rectifier, efficiency evaluation, loss analysis, and error compensation of inductor will be considered.

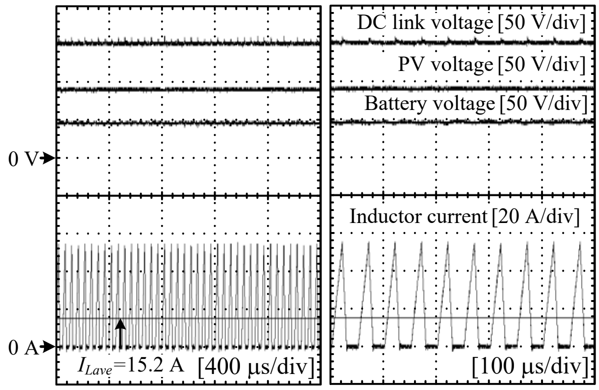

Fig. 7. Operation waveform of the Mode I.

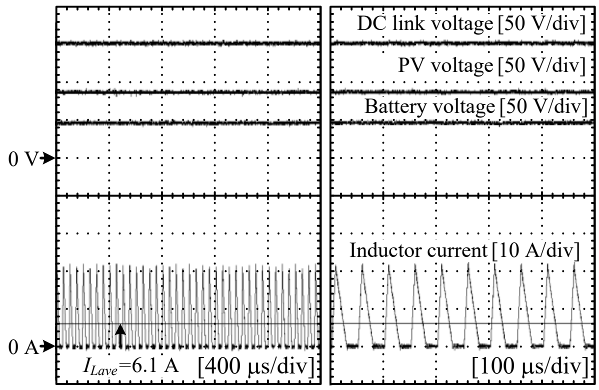

Fig. 8. Operation waveform of the Mode II.

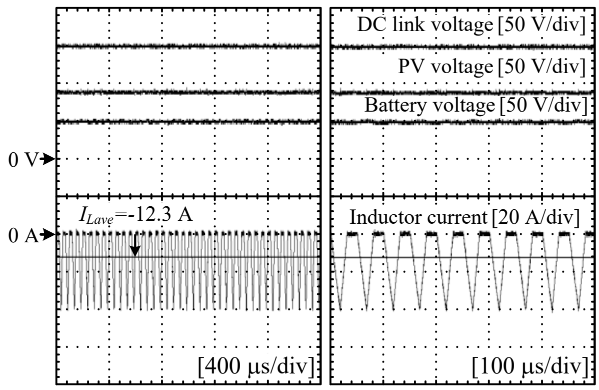

Fig. 9. Operation waveform of the Mode III.

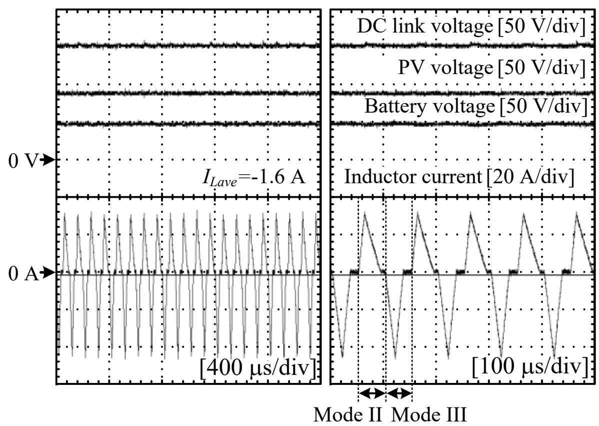

Fig. 10. Operation waveform of the Mode IV.

REFERENCES

[1] Keisuke Yamane, Daisuke Iioka, Hiroumi Saitoh: "Three - phase voltage control method by single-phase distributed generators connected to islanded distribution network", IEEJ transsactions on Power and Energy, vol. 139, No. 1, pp. 5–12(2019)

[2] Yona Atsushi, Uchida Kosuke, Senjyu Tomonobu, Funabashi Toshihisa : "Optimal Planning Strategy for Large PV/Battery System Based on Long-Term Insolation Forecasting", 2011 IEEJ transactions on Electronics, Information and Systems, vol. 131, pp. 1665-1671(2011)

[3] Endo Hiroaki, Yoshioka Yusuke, Inoue Kaoru, Kato Toshiji : "Grid Connection Point Power Factor Control based on the Level of Reverse Power Flow with a PV and Battery Power Conditioner" IEEJ Transactions on Industry Applications, vol. 139, pp. 51-59(2019)

[4] H. Mahmood, D. Michaelson and J. Jiang :"A Power Management Strategy for PV/Battery Hybrid Systems in Islanded Microgrids," in IEEE Journal of Emerging and Selected Topics in Power Electronics,vol. 2, no. 4, pp. 870-882, Dec. 2014.

[5] Amit Bhattacharjee, Nasser Kutkut, Issa Batarseh: "Review of Multi Port Converters for Solar and Energy Storage Integration", IEEE Transaction on Power Electronics, Vol.34, No.2, pp.1431-1445 (2019)

[6] H. Zhu, D. Zhang, B. Zhang and Z. Zhou:"A Nonisolated Three-Port DCDC Converter and Three-Domain Control Method for PV-Battery Power Systems", in IEEE Transactions on Industrial Electronics, vol.62, no. 8, pp. 4937-4947, (2015)

[7] K. Tomas-Manez, A. Anthon, Z. Zhang, Z. Ouyang and T. Franke: "High efficiency non-isolated three port DC-DC converter for PVbattery systems", 2016 IEEE 8th International Power Electronics and Motion Control Conference (IPEMC-ECCE Asia), pp.1806-1812,

[8] Xiaofeng Sun, Yue Zhou, Wei Wang, Baocheng Wang, Zhe Zhang : "Alternative Source-Port Tolerant Series-Connected Double-Input DC-DC Converter", IEEE Transaction on Power Electronics, Vol.30, No.5, pp.2733-2742 (2015)

[9] Koichi Matsuura, Jun-ichi Itoh: "A Loss Analysis of a 3-Level switched capacitor DC-DC Converter", SPC-11-098, PSE-11-061, PE11-044(2011)

[10] J. Itoh, K. Matsuura, K. Orikawa: "Reduction of a Boost Inductance using a Switched Capacitor DC-DC Converter", ICPE 2011 -ECCE Asia, pp. 1315-1322 (2011)

[11] H. N. Le, K. Orikawa, J. Itoh : "DCM Control Method of Boost Converter based on Conventional CCM Control", The 2014 International Power Electronics Conference, No. 21A4-5, pp. 3661-3666 (2014)

[12] Wm. T. Mclyman: "Transformer and inductor design handbook", Marcel Deller Inc. (2004)